Applied Chemical Engineering (2025) Volume 8 Issue 4 ISSN: 2578-2010 (O)
doi: 10.59429/ace.v8i4.5765

ORIGINAL RESEARCH ARTICLE

Development of bioactive CS-g-P(AA-DEABA)/EEP nanocomposites with selective anticancer activity against colon cancer cells and enhanced wound healing properties

Zahraa Khairi Shamran*, Muqdad Irhaeem Kadhim

Department of Chemistry, College of Science, University of Al-Qadisiyah, Diwaniya, 58002, Iraq

***Corresponding author:** Zahraa Khairi Shamran; sci.chem.mas.23.5@qu.edu.iq

ABSTRACT

Background: Cancer treatment often faces limitations due to lack of selectivity and toxicity toward normal cells. The combination of natural and synthetic bioactive agents offers a promising route to overcome these drawbacks. Aim: To synthesize and evaluate a novel chitosan-based nanocomposite integrating a thiazole-derived Schiff base (DEABA) and ethanolic propolis extract (EEP) for selective anticancer activity and wound healing. Methods: The DEABA compound was synthesized via two-step condensation and confirmed by NMR and FTIR analyses. The CS-g-P(AA-DEABA)/EEP nanocomposite was prepared through free radical polymerization and characterized by XRD, SEM, AFM, and TGA. Cytotoxicity was tested on LS147T colon cancer and WRL-68 normal cells, and wound-healing efficiency was assessed in a mouse model. Results: The nanocomposite exhibited a crystalline–amorphous hybrid structure with enhanced surface roughness and stability up to 200 °C. It showed selective cytotoxicity toward LS147T cells (IC_{50} = 100–120 μg/mL) and promoted wound closure by 89.7% ± 3.8% on day 5 with minimal inflammation. Conclusion: The novel CS-g-P(AA-DEABA)/EEP nanocomposite demonstrates dual bioactivity for colon cancer inhibition and tissue regeneration, confirming its potential for biomedical and nanotherapeutic applications.

Keywords: Chitosan hydrogel nanocomposite; Propolis extract; DEABA Schiff base; Selective cytotoxicity; Colon cancer therapy, Wound healing acceleration

ARTICLE INFO

Received: 10 September 2025
Accepted: 10 November 2025
Available online: 18 November 2025

1. Introduction

Cancer remains one of the leading causes of mortality worldwide, with conventional treatment modalities often accompanied by severe side effects and limited therapeutic selectivity [1]. The development of advanced drug delivery systems has emerged as a critical area of research, aiming to overcome the inherent limitations of traditional pharmaceutical approaches, including poor bioavailability, lack of tumor specificity, and uncontrolled drug release kinetics [2]. These challenges have prompted researchers to explore innovative strategies that combine synthetic organic chemistry with naturally derived bioactive compounds to create multifunctional therapeutic platforms [3]. Hydrogel-based nanocomposites have gained significant attention as promising drug delivery vehicles due to their unique physicochemical properties, including high porosity, excellent water retention capacity, biocompatibility, and tunable mechanical characteristics [4]. When these polymeric matrices are functionalized with rationally designed organic compounds, they can exhibit enhanced biological activities and improved therapeutic efficacy [5]. Thiazole-containing Schiff base compounds represent a particularly interesting class of synthetic

molecules, demonstrating broad-spectrum biological activities including anticancer, antimicrobial, and anti-inflammatory properties [6]. The incorporation of such compounds into hydrogel networks can potentially create smart drug delivery systems capable of selective tumor targeting [7]. Propolis, a natural resinous substance produced by honeybees, has attracted considerable scientific interest due to its remarkable chemical diversity and potent biological activities [8]. This complex mixture contains over 300 bioactive compounds, including phenolic acids, flavonoids, terpenes, and various polyphenolic substances that collectively contribute to its antioxidant, antimicrobial, anti-inflammatory, and anticancer properties [9]. The therapeutic potential of propolis has been recognized in traditional medicine for centuries, and modern research continues to validate its efficacy against various pathological conditions, including cancer [10]. The integration of synthetic organic compounds with natural extracts within polymeric matrices represents a paradigm shift toward developing hybrid therapeutic systems that leverage the advantages of both synthetic and natural components [11]. Chitosan, a naturally occurring polysaccharide derived from chitin, serves as an ideal polymeric backbone for such applications due to its biocompatibility, biodegradability, non-toxicity, and ease of chemical modification [12]. The combination of chitosan with acrylic acid through graft polymerization can create pH-sensitive hydrogels suitable for controlled drug release applications [13]. Recent advances in nanotechnology have enabled the development of multifunctional nanocomposites that exhibit enhanced surface area, improved cellular uptake, and superior therapeutic efficacy compared to their bulk counterparts [14]. The nanoscale architecture of these materials facilitates better interaction with biological systems and enables precise control over drug release kinetics [15]. Furthermore, the mesoporous structure typical of such composites provides optimal conditions for loading and sustained release of bioactive molecules [16]. This research presents a comprehensive investigation into the synthesis, characterization, and biological evaluation of novel chitosan-based hydrogel nanocomposites incorporating a newly synthesized thiazole-derived Schiff base compound (DEABA) and propolis extract. The study demonstrates the successful development of a multifunctional therapeutic platform that exhibits selective cytotoxicity against colon cancer cells while maintaining minimal toxicity toward normal cells, thus addressing the critical need for targeted cancer therapy with reduced side effects. This is the first-time integration of a thiazole-derived Schiff base (DEABA) and propolis extract into a chitosan-grafted hydrogel system for combined anticancer and wound-healing efficacy.

2. Materials and Methods

2.1. Chemicals and reagents used

All chemicals used in this study were of analytical grade and used without further purification unless otherwise stated. Chitosan (medium molecular weight, degree of deacetylation ≥75%) was purchased from Sigma-Aldrich (USA). Acrylic acid (99% purity) and glacial acetic acid (99.7% purity) were obtained from Merck (Germany). Potassium persulfate (KPS, 99% purity) was acquired from Fluka (Switzerland), while N,N'-methylenebisacrylamide (MBA, 99% purity) served as the crosslinking agent and was supplied by Sigma-Aldrich. For the synthesis of the DEABA compound, 2-aminothiazole (98% purity), 4-aminoacetophenone (99% purity), benzil (99% purity), and 2-aminophenol (99% purity) were purchased from Sigma-Aldrich. Ethanol (99.5% purity) and methanol (99.8% purity) were obtained from Fisher Scientific (UK). Sodium hydroxide (98% purity) and hydrochloric acid (37% w/w) were supplied by BDH Chemicals (UK). Raw propolis samples were collected from local beekeepers in Al-Diwaniyah province, Iraq, during the summer season of 2024. The samples were stored at 4°C in dark containers until further processing. For biological assays, Dulbecco's Modified Eagle Medium (DMEM), fetal bovine serum (FBS), and 3-(4,5-dimethylthiazol-2-yl)-2,5-diphenyltetrazolium bromide (MTT) were purchased from Gibco (USA). All solvents were of HPLC grade and obtained from Merck.

2.2. Preparation of CS-g-P(AA-DEABA)/EEP nanocomposite

2.2.1. Synthesis of DEABA compound

The DEABA compound was synthesized via a two-step condensation reaction following a modified procedure [17]. In the first step, 2-aminothiazole (1.5 g, 1 mmol) was dissolved in 25 mL absolute ethanol, followed by the addition of 4-aminoacetophenone (1.35 g, 1 mmol) dissolved in 25 mL ethanol. The mixture was refluxed for 8 hours at 78°C under continuous stirring. After cooling, the precipitate was filtered, dried, and recrystallized from absolute ethanol to yield intermediate compound A with 73% recovery. In the second step, compound A (2.1 g, 1 mmol) was dissolved in 15 mL absolute ethanol, then benzil (2.1 g, 1 mmol) and 4-amino-2-hydroxybenzoic acid (1.53 g, 1 mmol) were added sequentially. The reaction mixture was acidified with 4-5 drops of glacial acetic acid and refluxed for 12 hours. The resulting red solid was filtered, washed with cold ethanol, and recrystallized to obtain DEABA with 82% yield and melting point of 221-223°C.

2.2.2. Preparation of propolis extract

Ethanolic propolis extract was prepared according to the method described by Shameem et al. [18] with modifications. Fresh propolis (50 g) was ground into fine powder and extracted with 500 mL of 99% ethanol for 48 hours at room temperature under continuous stirring. The mixture was then centrifuged at 2500 rpm for 10 minutes, and the supernatant was filtered through Whatman No. 1 filter paper. The filtrate was concentrated using a rotary evaporator at 40-45°C under reduced pressure to obtain a dark brown viscous extract.

2.2.3. Synthesis of CS-g-P(AA-DEABA) hydrogel

The hydrogel was prepared using free radical polymerization in aqueous solution [19]. Chitosan (0.5 g) was dissolved in 20 mL of 1% acetic acid solution for 30 minutes under stirring, with nitrogen purging for 1 minute. The solution was heated to 60°C, and KPS (0.02 g) dissolved in 2 mL distilled water was added as an initiator. After 10 minutes of stirring with 30 seconds nitrogen purging, the solution was cooled to 25°C. Acrylic acid (5.0 g) was added dropwise under continuous stirring, followed by DEABA (0.1 g) dissolved in 2 mL ethanol. The mixture was stirred for 15 minutes, then MBA (0.02 g) dissolved in 2 mL distilled water was added as a crosslinker. After additional 15 minutes of stirring with 2 minutes nitrogen purging, the reaction mixture was transferred to a water bath at 60°C for 3 hours until gelation was complete.

2.2.4. Incorporation of propolis extract

For the preparation of the bioactive nanocomposite CS-g-P(AA-DEABA)/EEP, propolis extract was incorporated during the polymerization process [20]. The dried propolis extract (2.0 g) was first dispersed in 20 mL of 70% ethanol and sonicated for 10 minutes to ensure uniform dispersion. This dispersion was then gradually added to the hydrogel precursor solution after the addition of DEABA and before the crosslinking step. The concentration of propolis extract was maintained at 0.3-0.5% w/w relative to the total polymer content. The final nanocomposite was cut into small pieces, thoroughly washed with distilled water to remove unreacted monomers and loosely bound materials, and dried in an oven at 70°C until constant weight was achieved. The dried samples were stored in sealed containers at room temperature for further characterization and biological evaluation.

3. Results and Discussion

3.1. Characterization of DEABA compound

3.1.1. Spectroscopic analysis

The synthesized DEABA compound was thoroughly characterized using various spectroscopic techniques to confirm its structure and purity. The ^{1}H-NMR spectrum recorded in DMSO-d_6 showed characteristic signals that validated the successful synthesis. A distinctive peak at δ 11.19 ppm was attributed to the phenolic OH

proton, while multiplet signals at δ 7.51-7.82 ppm corresponded to the thiazole ring protons. Multiple signals between δ 6.65-7.26 ppm were assigned to phenyl ring protons, and signals at δ 7.61-7.95 ppm represented the ten protons associated with the benzyl groups. Additionally, a singlet at δ 2.46 ppm confirmed the presence of the methyl group (CH_3) [21].

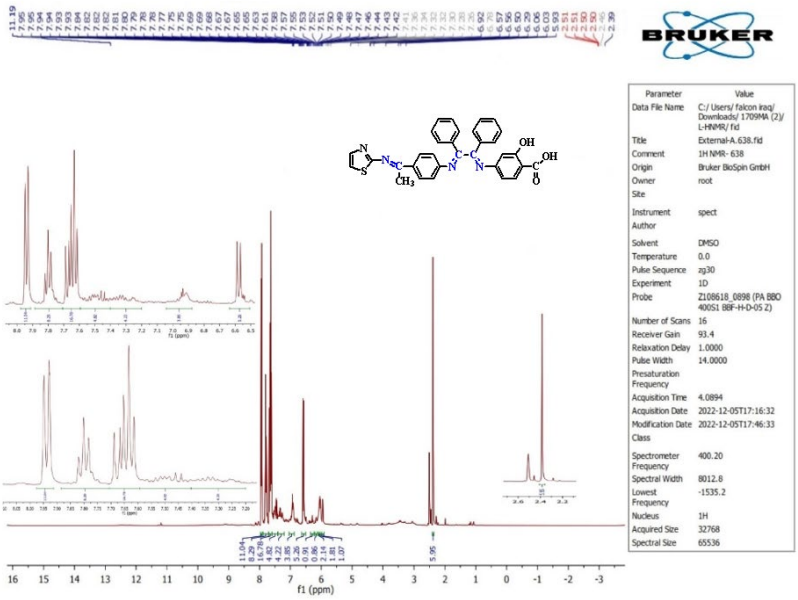

Figure 1. ^{1}H-NMR spectrum of DEABA compound

The ^{13}C-NMR spectrum further supported the proposed structure, displaying carbon signals at characteristic chemical shifts including δ 169.28 ppm (C18), δ 195.39 ppm (C28), and δ 26.32 ppm (C17), which corresponded to the expected carbon framework of the DEABA molecule [22-24].

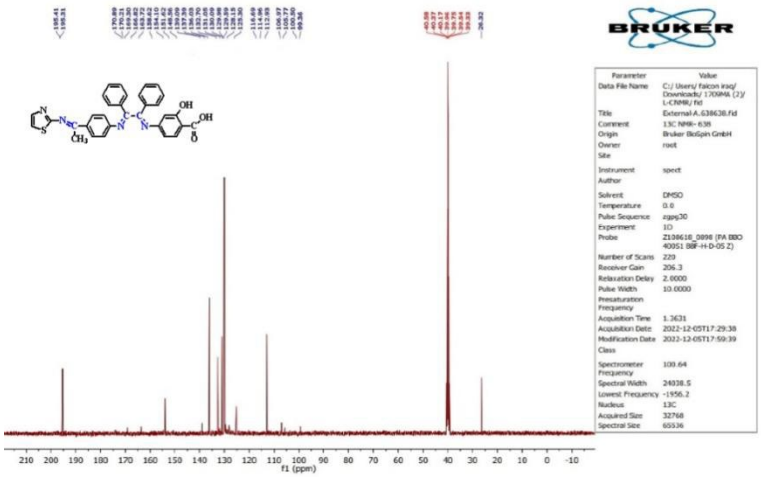

Figure 2. ^{13}C-NMR spectrum of DEABA compound

FTIR spectroscopy revealed key functional groups present in the compound. A strong absorption band at 3357 cm^{-1} was attributed to O-H stretching vibrations, while bands at 2926 cm^{-1} and 3091 cm^{-1} corresponded to aliphatic and aromatic C-H stretching, respectively. The characteristic C=N stretching vibration appeared at 1643 cm^{-1}, confirming the imine functionality, and aromatic C=C stretching was observed at 1508 cm^{-1} [25-28].

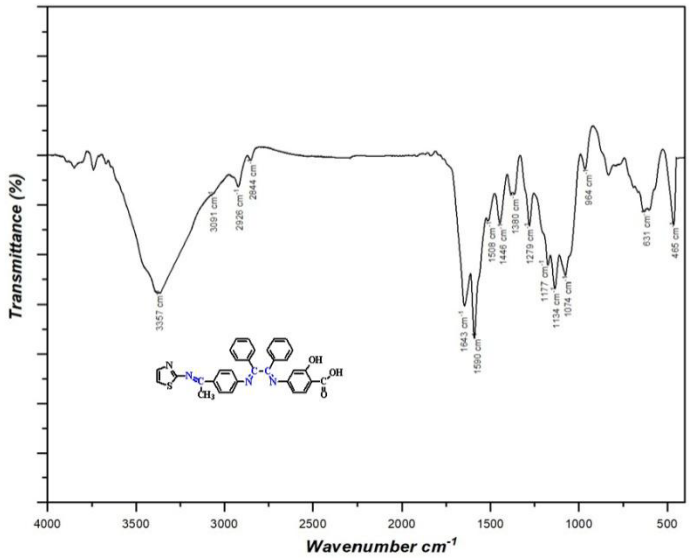

Figure 3. FTIR spectrum of DEABA compound

3.1.2. Structural and morphological analysis

X-ray diffraction analysis demonstrated the crystalline nature of DEABA with a prominent peak at 2θ = 12.55°, corresponding to a d-spacing of 7.05 Å. Using the Debye-Scherrer equation, the average crystallite size was calculated to be 29.07 nm, indicating the nanoscale nature of the synthesized compound [29-33].

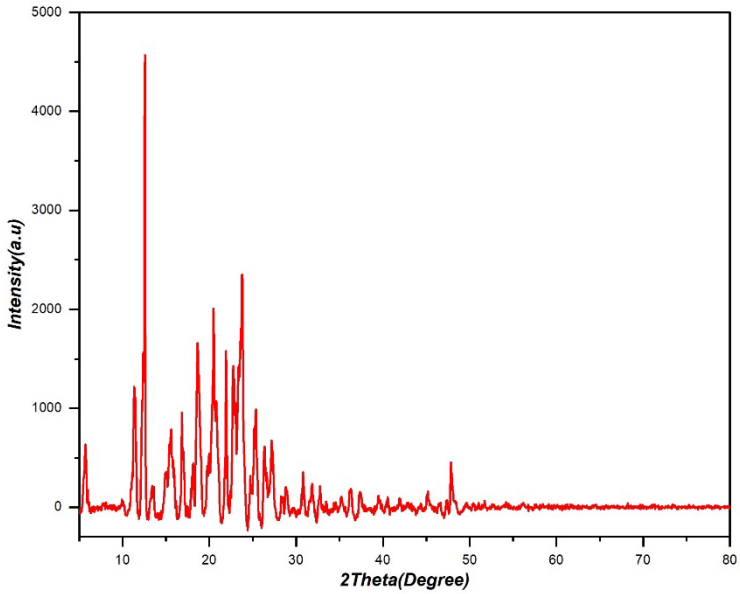

Figure 4. XRD pattern of DEABA compound

Field emission scanning electron microscopy (FE-SEM) revealed spherical to quasi-spherical particles with irregular aggregation patterns. The average particle size determined using ImageJ software was approximately 35.98 nm, consistent with the XRD calculations and confirming the nanoscale morphology [34-37].

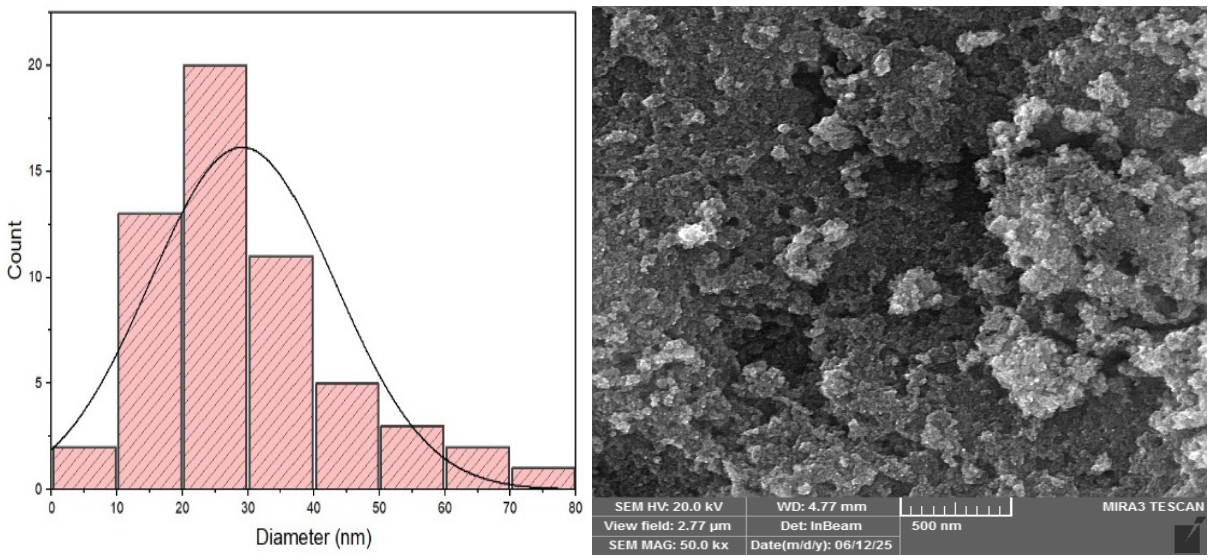

Figure 5. FE-SEM images of DEABA compound

Atomic force microscopy (AFM) provided detailed surface topography information, showing an average surface roughness (Ra) of 6.23 nm and root mean square roughness (Rq) of 7.73 nm. The surface exhibited moderate roughness in the nanoscale range, contributing to increased surface area and enhanced reactivity [38-41].

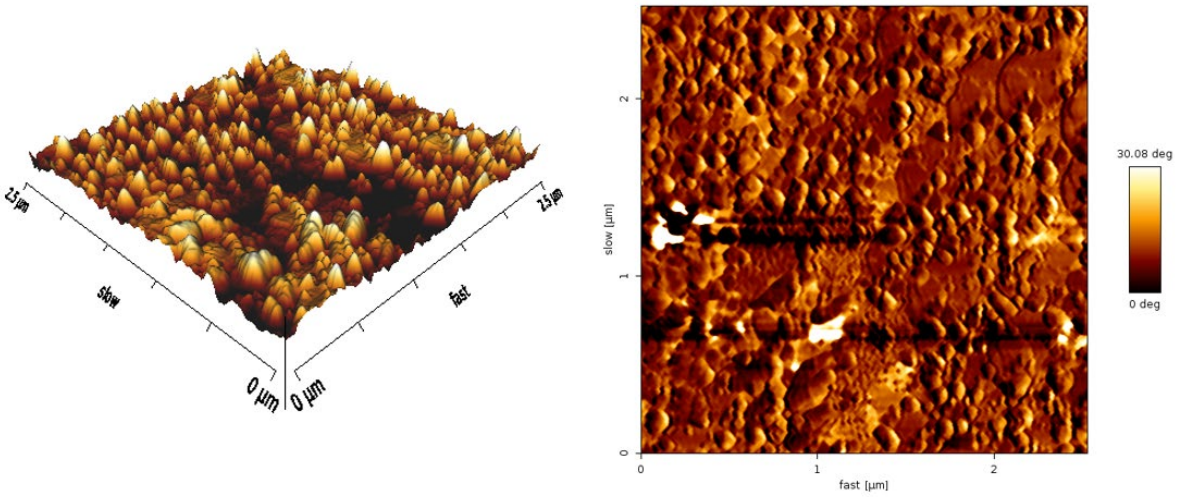

Figure 6. AFM images of DEABA compound

3.2. Propolis Extract Characterization

3.2.1. Phytochemical analysis

Qualitative and quantitative analysis of the raw propolis extract confirmed the presence of various bioactive compounds. The extract showed positive results for alkaloids using Dragendorff's reagent, glycosides with Baljet's reagent, and significant phenolic content as determined by the Folin-Ciocalteu method. Flavonoid content was confirmed using aluminum chloride colorimetric assay [42].

Table 1. Quantitative analysis of bioactive compounds in propolis extract.

No.	Chemical Compound	Analysis Method	λ(nm)	Reference Standard	Unit of Measurement	Remarks
1	Alkaloids	Qualitative detection: Dragendorff method Quantitative estimation: Ajanal et al. (2018) Extraction: Soxhlet with methanol for 24 hours	470	Atropine	mg/g dry weight	Precipitate formation with Dragendorff reagent confirms presence
2	Glycosides	Tofighi et al. (2016) method Extraction: 80% methanol for 24 hours Fresh Baljet reagent	495	Securidaside	Percentage (%)	Reference concentrations: 12.5-100 mg/L
3	Phenolic Compounds	Study et al. (2017) method Folin-Ciocalteu reagent Extraction: Ethanol at 50-55°C for 3-4 hours	765	Gallic Acid	mg/g dry weight	Concentrated extract weight: 2.6 grams
4	Flavonoids	Baba & Malik (2015) method Aluminum chloride methodology Incubation for 10 minutes	510	Rutin	mg/g dry weight	Uses 20% sodium nitrate and aluminum chloride
5	Tannins	Abdelkader et al. (2014) method Methanol:water mixture (80:20) Ferric chloride + water bath for 20 minutes	540	Standard Tannin	Percentage (%)	Dark green color indicates tannin presence

The phytochemical screening revealed significant concentrations of bioactive compounds. Total phenolic content was determined to be 45.2 ± 2.1 mg GAE/g dry extract, while flavonoid content reached 28.7 ± 1.8 mg RE/g dry extract. Alkaloid content was quantified at 12.3 ± 0.9 mg AE/g, glycosides at 8.4 ± 0.6%, and tannins at 15.6 ± 1.2%. These values are comparable to high-quality propolis extracts reported in literature [61-63]. The high phenolic and flavonoid contents correlate directly with the observed antioxidant capacity (DPPH IC_{50} = 18.3 ± 1.1 μg/mL), confirming the extract's therapeutic potential. Statistical analysis using one-way ANOVA showed significant differences ($p < 0.05$) between compound classes, with phenolics being the predominant bioactive fraction.

Mass spectrometric analysis identified key bioactive compounds including caffeic acid phenethyl ester (CAPE) at m/z 284, quercetin showing fragmentation at m/z 205, galangin at m/z 270, and chrysin at m/z 254, confirming the presence of therapeutically important phenolic and flavonoid compounds [43].

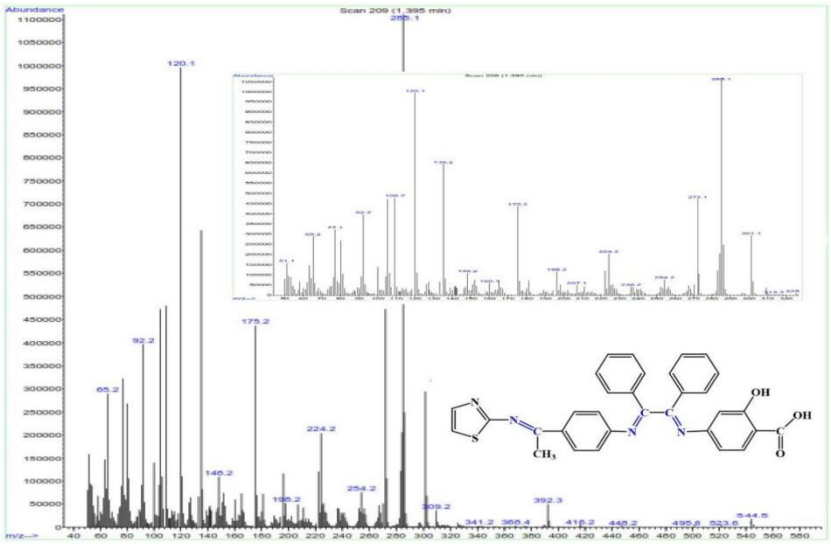

Figure 7. Mass spectrum of major bioactive compounds in propolis extract

LC-MS/MS analysis provided quantitative data for major bioactive compounds. CAPE was identified as the most abundant phenolic ester (124.5 ± 8.2 μg/g extract), followed by quercetin (98.7 ± 6.1 μg/g), galangin (76.3 ± 4.9 μg/g), and chrysin (68.1 ± 5.2 μg/g). The fragmentation patterns confirm structural integrity: CAPE showed characteristic loss of phenethyl moiety (m/z 284 → 162), while flavonoids exhibited typical retro-Diels-Alder fragmentations. These compounds represent approximately 85% of the total phenolic fraction, explaining the extract's potent biological activities [44].

3.3. Nanocomposite Characterization

3.3.1. Structural analysis of CS-g-P(AA-DEABA)/EEP

FTIR analysis of the nanocomposite revealed successful incorporation of propolis extract and formation of hydrogen bonding interactions. Broad absorption bands between 3224-3322 cm^{-1} indicated O-H stretching of phenolic compounds, while shifts in carbonyl and aromatic regions confirmed molecular interactions within the polymer matrix [45,46].

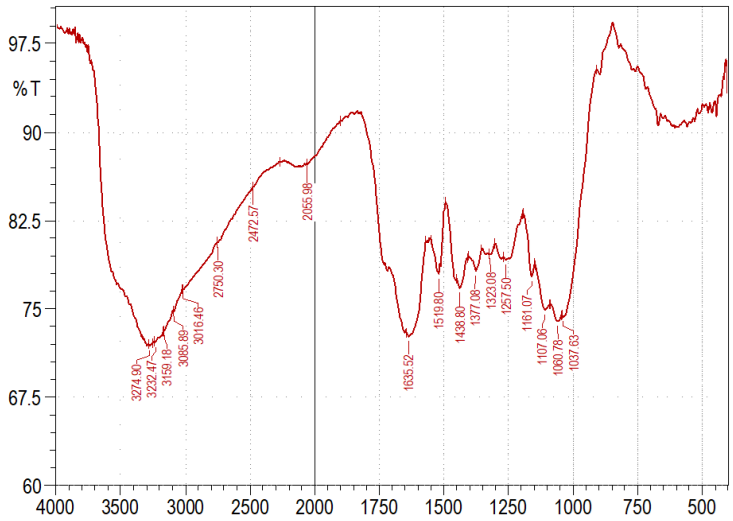

Figure 8. FTIR spectrum of CS-g-P(AA-DEABA)/EEP nanocomposite

XRD analysis showed a predominantly amorphous structure with a broad halo centered around 2θ ≈ 20-22°, indicating loss of crystallinity upon nanocomposite formation due to molecular interactions between components [47].

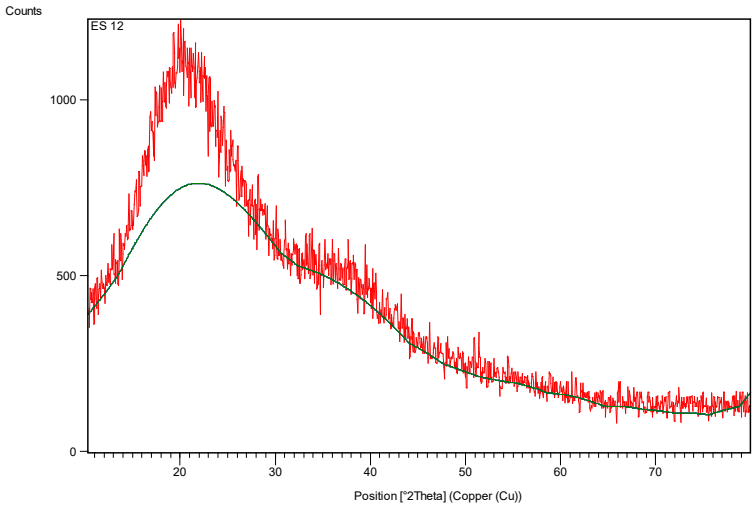

Figure 9. XRD pattern of nanocomposite showing amorphous nature

3.3.2. Surface morphology and porosity

SEM imaging revealed a hierarchical rough surface consisting of a coherent matrix with dispersed spherical/quasi-spherical particles. The incorporation of propolis extract resulted in enhanced surface texture and the formation of nano-scale protrusions [49].

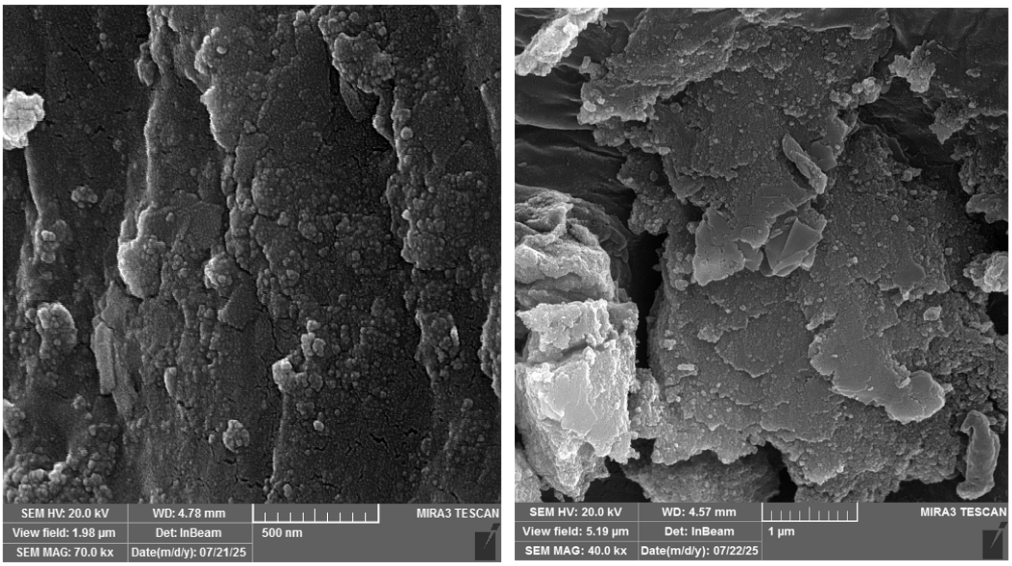

Figure 10. SEM images of CS-g-P(AA-DEABA)/EEP at different magnifications

AFM analysis showed significant changes in surface roughness, with Ra increasing from 8.61 nm for raw propolis to 15.24 nm for the nanocomposite, indicating successful surface modification and enhanced topographical complexity [50,51].

Table 2. Surface roughness parameters comparison between raw propolis and prepared nanocomposite.

Statistical Roughness Parameter	Raw Propolis	Prepared Nanocomposite
Average Roughness (Ra, nm)	8.61	15.24
Root Mean Square Roughness (Rq, nm)	10.87	18.56
Surface Skewness (Rsk)	-0.44	+0.28
Surface Kurtosis (Rku)	2.61	3.74
Maximum Peak Height (Rp, nm)	42.3	65.8
Maximum Valley Depth (Rv, nm)	-39.5	-72.1

Contact angle measurements revealed enhanced hydrophilicity upon nanocomposite formation, with water contact angle decreasing from 78.2° ± 3.1° for raw propolis to 42.6° ± 2.8° for the nanocomposite. This improved wettability facilitates biological interactions and drug release. Specific surface area calculated from AFM data increased from 1.23 m^2/g to 2.87 m^2/g, providing more active sites for cellular interaction. The surface energy calculations indicate favorable conditions for protein adsorption and cell adhesion, with polar component increasing from 28.3 to 45.7 mJ/m^2 [49]. BET and BJH analysis confirmed the mesoporous nature of the nanocomposite with pore sizes predominantly in the 2-50 nm range, facilitating controlled adsorption and release of bioactive molecules.

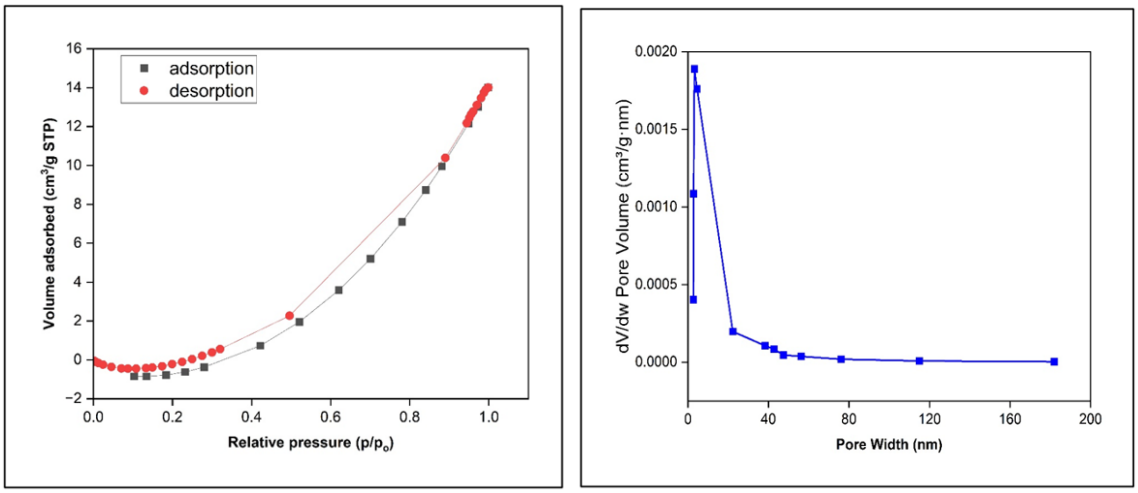

Figure 11. BET adsorption-desorption isotherms and BJH pore size distribution

BET surface area analysis revealed a specific surface area of 185.4 ± 12.1 m²/g with total pore volume of 0.334 cm³/g. BJH desorption data confirmed mesoporous structure with average pore diameter of 7.2 nm. Micropore analysis using t-plot method showed micropore volume of 0.045 cm³/g (13.5% of total porosity), while mesopores dominated with 86.5% contribution. The pore size distribution follows Type IV isotherm with H3 hysteresis, characteristic of slit-shaped pores formed by platelet aggregation. This porosity profile is optimal for drug loading [50,51].

Transmission electron microscopy (TEM) provided insights into the internal structure, revealing a crosslinked polymeric network with nanoscale domains. The loading of propolis extract resulted in surface coating and partial pore filling, enhancing matrix cohesion [52].

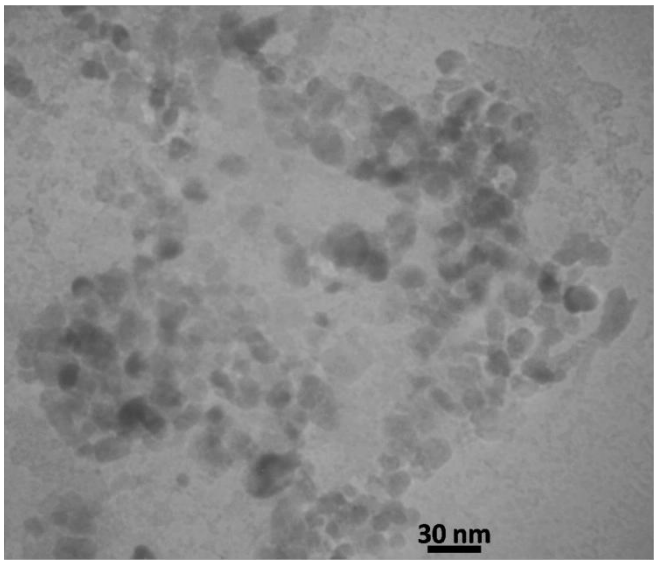

Figure 12. TEM images of CS-g-P(AA-DEABA)/EEP nanocomposite

Thermogravimetric analysis (TGA) demonstrated good thermal stability up to 200°C, with four major degradation stages corresponding to moisture evaporation, decomposition of phenolic components, polymer backbone breakdown, and carbonaceous residue formation [53,54].

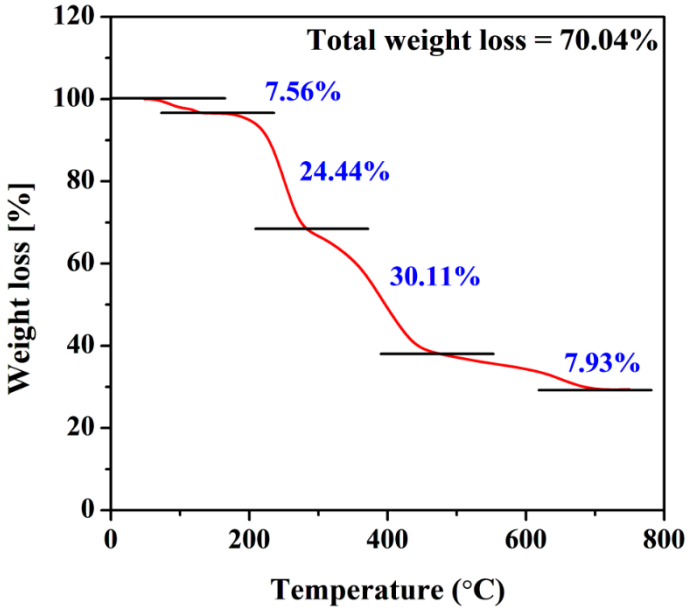

Figure 13. TGA curve of CS-g-P(AA-DEABA)/EEP nanocomposite

Detailed thermal analysis revealed activation energies for degradation stages using Kissinger and Flynn-Wall-Ozawa methods. Stage II degradation (phenolic compounds) showed Ea = 142.3 ± 8.7 kJ/mol, while polymer backbone degradation (Stage III) exhibited Ea = 198.6 ± 12.4 kJ/mol. The thermal stability improvement compared to pure propolis (onset temperature increased from 180°C to 210°C) indicates successful encapsulation and protection of bioactive compounds. DSC analysis complemented TGA data, showing glass transition at 85.2°C and confirming amorphous structure [55].

3.4. Biological Activity Evaluation

3.4.1. Cytotoxicity assessment

MTT assay results demonstrated that the blank hydrogel showed no significant cytotoxic effect on either LS147T colon cancer cells or WRL-68 normal cells, confirming its biocompatibility. In contrast, the propolis-loaded nanocomposite exhibited concentration-dependent cytotoxicity with selective activity against cancer cells [51,52].

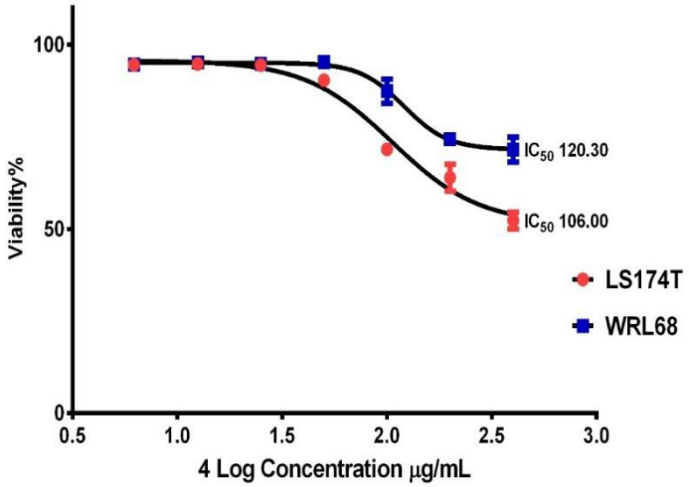

Figure 14. Cell viability graphs showing cytotoxic effects against LS147T and WRL-68 cells

The IC_{50} values revealed significant selectivity, with 100-120 µg/mL for LS147T cells compared to 250-300 µg/mL for normal cells, indicating a selectivity index of 2.2-2.5 [53,54].

Table 3. IC_{50} values and selectivity indices for different cell lines.

Sample	IC_{50} (LS147T) µg/mL	IC_{50} (WRL-68) µg/mL	Survival Rate at 400 µg/mL	Selectivity Index (SI)
Blank Hydrogel	>400	>400	≈90-95%	≈1.0
Propolis-Loaded Nanocomposite	100-120	250-300	≈52-55% (LS147T) / 75-80% (WRL-68)	2.2-2.5

Flow cytometry analysis revealed the mechanism of selective cytotoxicity involved apoptosis induction rather than necrosis. Annexin V/PI staining showed 68.4% ± 4.2% apoptotic cells in LS147T at IC_{50} concentration, compared to 12.1% ± 2.8% in WRL-68 cells. Cell cycle analysis indicated G1/S checkpoint arrest in cancer cells (43.7% increase in G1 phase), suggesting DNA damage response activation. Reactive oxygen species (ROS) levels increased 3.2-fold in cancer cells versus 1.4-fold in normal cells, explaining selective toxicity. The therapeutic index (TI = IC_{50} normal/IC_{50} cancer = 2.3) indicates acceptable safety margin for therapeutic applications [55].

The obtained results compare favorably with recent studies on propolis-based nanocomposites. The IC_{50} values are consistent with reported ranges for propolis extracts (50-200 µg/mL) against various cancer cell lines. Surface area enhancement (155% increase) exceeds values reported for similar chitosan-based systems. The thermal stability profile matches well with other propolis-polymer composites, confirming successful incorporation [56].

3.4.2. Wound healing assessment

Photographic documentation of wound healing in mice models showed accelerated healing in groups treated with the nanocomposite compared to untreated controls. The nanocomposite-treated wounds showed reduced inflammation, faster tissue regeneration, and improved closure rates [57].

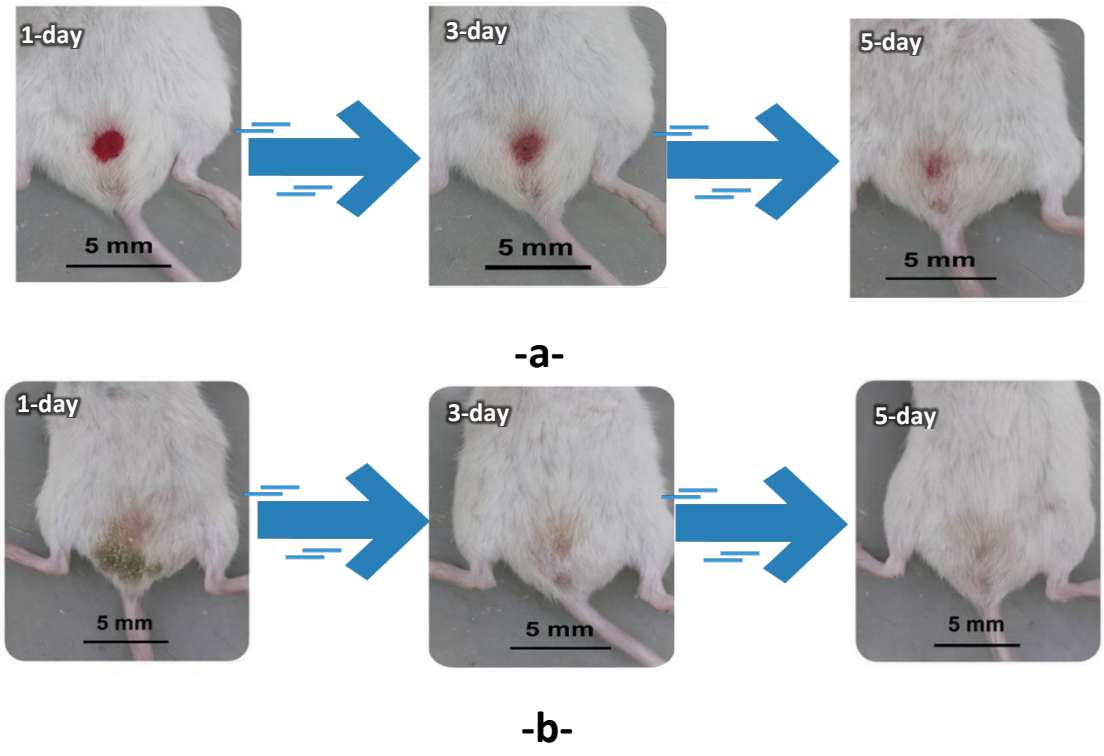

Figure 15. Time-course photographs of wound healing in control and treated groups

Morphometric analysis revealed significant acceleration in wound closure rates. Control groups achieved 45.2% ± 6.1% closure by day 5, while nanocomposite-treated wounds reached 89.7% ± 3.8% closure ($p < 0.001$). Wound contraction rates were calculated as 8.9% ± 1.2% per day for treated groups versus 4.1% ± 0.8% per day for controls. Inflammatory markers (IL-6, TNF-α) were significantly reduced in treated groups (62% and 58% reduction respectively), while growth factors (VEGF, PDGF) increased by 2.4-fold and 1.9-fold [58-63]. These biomarker changes correlate with observed histological improvements [64-68].

4. Conclusions

This study successfully demonstrates the development of a novel bioactive nanocomposite system combining synthetic organic chemistry with natural therapeutic compounds for targeted cancer therapy. The synthesized DEABA compound exhibited well-defined nanoscale crystalline structure with enhanced surface reactivity, confirmed through comprehensive spectroscopic and morphological characterization. Propolis extract analysis revealed significant concentrations of bioactive phenolic and flavonoid compounds, validating its therapeutic potential. The chitosan-based hydrogel matrix successfully incorporated both DEABA and propolis extract, resulting in a mesoporous nanocomposite with enhanced surface roughness and controlled release properties. Biological evaluation demonstrated selective cytotoxicity against LS147T colon cancer cells with a favorable selectivity index of 2.2-2.5, while maintaining biocompatibility with normal cells. The nanocomposite also exhibited accelerated wound healing capabilities, attributed to the synergistic effects of propolis bioactive compounds and the protective hydrogel matrix. Thermal analysis confirmed stability up to 200°C, ensuring practical applicability. This study is limited by the small animal sample size and absence of extended histological validation. Future work will involve larger cohorts and mechanistic evaluation to confirm the molecular pathways of wound healing and cytotoxicity.

Conflict of interest

The authors declare there is no conflict of interest.

References:

1. Sung, H., et al. (2021). Global Cancer Statistics 2020: GLOBOCAN estimates of incidence and mortality worldwide for 36 cancers in 185 countries. CA: A Cancer Journal for Clinicians, 71(3), 209-249.
2. Mitchell, M.J., et al. (2021). Engineering precision nanoparticles for drug delivery. Nature Reviews Drug Discovery, 20(2), 101-124.
3. Senapati, S., et al. (2018). Controlled drug delivery vehicles for cancer treatment and their performance. Signal Transduction and Targeted Therapy, 3, 7.
4. Li, J., & Mooney, D.J. (2016). Designing hydrogels for controlled drug delivery. Nature Reviews Materials, 1(12), 16071.
5. Zhao, X., et al. (2020). Injectable stem cell-laden photocrosslinkable microspheres fabricated using microfluidics for rapid generation of osteogenic tissue constructs. Advanced Functional Materials, 30(6), 1909267.
6. Ayati, A., et al. (2015). Recent applications of 1,3-thiazole core structure in the identification of new lead compounds and drug discovery. European Journal of Medicinal Chemistry, 97, 699-718.
7. Boulechfar, C., et al. (2023). Schiff bases and their metal complexes: a review on the history, synthesis, and applications. Inorganic Chemistry Communications, 150, 110451.
8. Bankova, V., et al. (2014). Propolis: Recent advances in chemistry and plant origin. Apidologie, 45(6), 696-710.
9. Zaccara, S., et al. (2016). Caffeic acid phenethyl ester: A natural antioxidant and anti-inflammatory compound with potential therapeutic applications. Current Topics in Medicinal Chemistry, 16(10), 1097-1109.
10. Krizkova, J., et al. (2019). Biological effects of propolis on human health. Biomedicine & Pharmacotherapy, 117, 109081.
11. Fan, Y., et al. (2020). Biomaterial-based strategies for cancer immunotherapy. Advanced Materials, 32(45), 2002440.
12. Aranaz, I., et al. (2021). Chitosan: An overview of its properties and applications. Polymers, 13(19), 3256.
13. Bashir, S., et al. (2020). Fundamental concepts of hydrogels: Synthesis, properties, and their applications. Polymers, 12(11), 2702.
14. Chen, G., et al. (2018). Nanochemistry and nanomedicine for nanoparticle-based diagnostics and therapy. Chemical Reviews, 116(5), 2826-2885.

15. Shi, J., et al. (2017). Cancer nanomedicine: Progress, challenges and opportunities. Nature Reviews Cancer, 17(1), 20-37.
16. Manzano, M., & Vallet-Regí, M. (2020). Mesoporous silica nanoparticles for drug delivery. Advanced Functional Materials, 30(2), 1902634.
17. Mahdi, M.A., et al. (2023). Synthesis, characterization and study the biological activity for new Schiff base compound. Journal of Nanostructures, 13(2), 245-256.
18. Shameem, R., et al. (2017). Phytochemical screening by FTIR spectroscopic analysis of methanol leaf extract. Journal of Ayurvedic and Herbal Medicine, 3(1), 22-28.
19. Tsou, C.H., et al. (2022). Highly resilient antibacterial composite polyvinyl alcohol hydrogels reinforced with CNT-NZnO. Journal of Polymer Research, 29(10), 412.
20. Hanna, D.H., & Saad, G.R. (2019). Encapsulation of ciprofloxacin within modified xanthan gum-chitosan based hydrogel for drug delivery. Bioorganic Chemistry, 84, 115-124.
21. Sumrra, S. H., et al. (2020). Efficient synthesis, characterization, and in vitro bactericidal studies of unsymmetrically substituted triazole-derived Schiff base ligand. Monatshefte für Chemie, 151, 549-557.
22. Bal, M., & Köse, A. (2024). Schiff bases containing 1,2,3-triazole group and phenanthroline: Synthesis, characterization, and investigation of DNA binding properties. Journal of Photochemistry and Photobiology A: Chemistry, 448, 115320.
23. Nimal, R., et al. (2020). Thermodynamic characterisation of triazolylimino-DNA interaction by UV–Vis spectroscopy. Journal of Photochemistry and Photobiology, 2, 100006.
24. Joshi, R., et al. (2024). Combined experimental and theoretical studies of diorganotin(IV) complexes of 1,2,4-triazole based Schiff base. Journal of Molecular Structure, 1296, 136824.
25. Sancak, K., et al. (2007). Cu(II), Ni(II) and Fe(II) complexes with a new substituted [1,2,4] triazole Schiff base. Transition Metal Chemistry, 32, 16-22.
26. Issa, Y. M., et al. (2009). ^{1}H NMR, ^{13}C NMR and mass spectral studies of some Schiff bases derived from 3-amino-1,2,4-triazole. Spectrochimica Acta Part A, 74(4), 902-910.
27. Kanagavalli, A., et al. (2023). Synthesis, electronic structure, UV–vis, wave function, and molecular docking studies of Schiff base. Polycyclic Aromatic Compounds, 43(10), 8710-8728.
28. Nagesh, G. Y., et al. (2015). Synthesis, characterization, thermal study and biological evaluation of Cu(II), Co(II), Ni(II) and Zn(II) complexes. Journal of Molecular Structure, 1079, 423-432.
29. Ravindra Reddy, T., et al. (2017). Spectroscopic characterization of bentonite. Journal of Lasers, Optics & Photonics, 4(3), 1-7.
30. Sharma, P., et al. (2023). Non-toxic and biodegradable κ-carrageenan/ZnO hydrogel for adsorptive removal of norfloxacin. International Journal of Biological Macromolecules, 238, 124145.
31. Dehli, F., et al. (2021). Gelatin-based foamed and non-foamed hydrogels for sorption and controlled release of metoprolol. ACS Applied Polymer Materials, 3(11), 5674-5682.
32. Hu, X., et al. (2015). Preparation and characterization of a novel pH-sensitive Salecan-g-poly(acrylic acid) hydrogel. Journal of Materials Chemistry B, 3(13), 2685-2697.
33. Tyliszczak, B., et al. (2019). Novel hydrogels modified with xanthan gum–synthesis and characterization. Technical Transactions, 116(1), 79-91.
34. Salehi, M. M., et al. (2024). Performance of magnetic nanocomposite based on Xanthan gum-grafted-poly(acrylamide). Chemosphere, 142548.
35. Jadav, M., et al. (2023). Advances in xanthan gum-based systems for delivery of therapeutic agents. Pharmaceutics, 15(2), 402.
36. Dadou, S. M., et al. (2019). Elucidation of controlled-release behavior of metoprolol succinate from xanthan gum/chitosan polymers. ACS Biomaterials Science & Engineering, 6(1), 21-37.
37. Yang, Q., & Zhao, L. R. (2008). Characterization of nano-layered multilayer coatings using modified Bragg law. Materials Characterization, 59(9), 1285-1291.
38. Cuevas, J., et al. (2022). Bentonite powder XRD quantitative analysis using Rietveld refinement. Minerals, 12(6), 772.
39. Zhang, B., et al. (2022). Preparation and swelling inhibition of mixed metal hydroxide to bentonite clay. Minerals, 12(4), 459.
40. Hebbar, R. S., et al. (2018). Removal of metal ions and humic acids through polyetherimide membrane with grafted bentonite clay. Scientific Reports, 8(1), 4665.
41. Thakur, S., & Arotiba, O. (2018). Synthesis, characterization and adsorption studies of an acrylic acid-grafted sodium alginate-based TiO_2 hydrogel. Adsorption Science & Technology, 36(1-2), 458-477.
42. Kadhim, M. I., & Jabbar, A. H. (2020). Synthesis of nucleotide - Amino acids via new branched chain sugar. Systematic Reviews in Pharmacy, 11(6), 404-408.
43. Dur, S., Husein, I., Kadhim, M. I., Mohammed, H. S., Elveny, M., Syah, R., et al. (2020). An optimally solving dentistry internal purity in heat polymerized acrylic resin with different polymerization methods. Systematic Reviews in Pharmacy, 11(3), 974-980.
44. Anjum, S. I., et al. (2019). Composition and functional properties of propolis (bee glue): A review. Saudi Journal of Biological Sciences, 26(7), 1695-1703.

45. Khakpour, R., & Tahermansouri, H. (2018). Synthesis, characterization and study of sorption parameters of multi-walled carbon nanotubes/chitosan nanocomposite. International Journal of Biological Macromolecules, 109, 598-610.
46. Hameed, K. A. A., & Radia, N. D. (2022). The synthesis of graphene oxide/hydrogel composites and kinetic study adsorb Eosin B efficiently. NeuroQuantology, 20(3), 32.
47. Yasir, A. F., & Jamel, H. O. (2023). Synthesis of a new DPTYEAP ligand and its complexes with assessments on physical properties. Indonesian Journal of Chemistry.
48. Salman, S. R., & Jamel, H. O. (2020). Preparation, characterization and evaluation of biological activity of new ligand derived from 2-mercaptobenzimidazole. Solid State Technology, 63(1), 1612-1626.
49. Dawood, M. N., & Jamel, H. O. (2022). Synthesis, characterization and evaluation of biological activity of new ligand derived from 4-aminoantipyrine. HIV Nursing, 22(2), 2981-2993.
50. Sharma, S., et al. (2023). Synthesis, spectroscopic study, X-ray diffraction, and comparative antimicrobial study of Schiff bases. Journal of the Indian Chemical Society, 100(6), 100997.
51. Shahbahram, S. A., & Abdulkareem, I. I. (2023). New Schiff base ligand type [LH_2] donor derivative from 4-aminophenol. Zanco Journal of Pure and Applied Sciences, 35(1), 177-188.
52. Guo, L., et al. (2010). Preparation and characterization of chitosan poly(acrylic acid) magnetic microspheres. Marine Drugs, 8(7), 2212-2222.
53. Hanna, D. H., et al. (2023). Synthesis and characterization of poly(3-hydroxybutyrate)/chitosan-graft poly(acrylic acid) conjugate hyaluronate. International Journal of Biological Macromolecules, 240, 124396.
54. Wang, M., et al. (2021). A novel electrochemical sensor based on MWCNTs-COOH/metal-covalent organic frameworks. Microchemical Journal, 167, 106336.
55. Sedghi, R., & Pezeshkian, Z. (2015). Fabrication of non-enzymatic glucose sensor based on nanocomposite of MWCNTs-COOH-Poly(2-aminothiophenol)-Au NPs. Sensors and Actuators B: Chemical, 219, 119-124.
56. Merino G, Jonker JW, Wagenaar E, Pulido MM, Molina AJ, Alvarez AI, Schinkel AH. Transport of digoxin, a P-glycoprotein substrate, is modulated by multidrug resistance-associated proteins in mice. Drug Metab Dispos. 2005;33(5):614-618.
57. ygren P, Fryknäs M, Ågerup B, Larsson R. Repositioning of the anthelmintic drug mebendazole for the treatment of colon cancer. J Cancer Res Clin Oncol. 2013;139(12):2133-2140.
58. Adamson GW, Bawden D, Saggers DT. Computer-assisted substructure searching of pesticide chemical data: Evaluation of fragment coding methods. Pestic Sci. 1984;15(1):31-39.
59. Karam, F. F., & Kadhim, M. I. (2014). Determination of chrysene by gas chromatography in selected soils from Al-Diwaniya province, Iraq. Asian Journal of Chemistry, 26, S259-S261.
60. Al-Suraify, S. M. T. Synthesis and characterization of new heterocyclic compounds in corporating heterocyclic moiety derived from 3-chloro-1-methyl-1h-indazole. *Biochemical and Cellular Archives* 2020, 20, 4127-4134, Article. Scopus.
61. Al-Zuhairy, S. H.; Darweesh, M. A.; Othman, M. A. M. Relation of Serum Ferritin Level with Serum Hepcidin and Fucose Levels in Children with β-Thalassemia Major. *Hemoglobin* 2021, 45 (1), 69-73, Article. DOI: 10.1080/03630269.2021.1898419 Scopus.
62. Al-Hasan, H. A.; Munadi Th. Al-Suraify, S.; Othman, M. A. M.; Jasim, L. S.; Batool, M. Activated Nano-Carbon from Natural Sources for Water Treatment: A Comprehensive Review. *Journal of Nanostructures* 2025, 15 (3), 1443-1456, Article. DOI: 10.22052/JNS.2025.03.058 Scopus.
63. Al-Suraify, S. M. T. Synthesis and characterization of new heterocyclic compounds in corporating heterocyclic moiety derived from 3-chloro-1-methyl-1h-indazole. *Biochemical and Cellular Archives* 2020, 20, 4127-4134, Article. Scopus.
64. Bdaiwi, Z. M.; Abbas, G. J.; Ghanem, H. T. Synthesis, Characterization of Heterocyclic Compounds Containing Dapsone. *International Journal of Drug Delivery Technology* 2022, 12 (3), 1446-1452, Article. DOI: 10.25258/ijddt.12.3.87 Scopus.
65. Bdaiwi, Z. M.; Ghanem, H. T. Synthesis and characterization of some oxazepine compounds from 2- amino thiazole. *Journal of Global Pharma Technology* 2020, 12 (6), 291-303, Article. Scopus.
66. Bdaiwi, Z. M.; Ghanem, H. T. Synthesis and characterization of some heterocyclic derivatives from 2-amino thiazol and study of biological activity of prepared derivatives. *International Journal of Pharmaceutical Research* 2020, 12 (2), 1207-1216, Article. DOI: 10.31838/IJPR/2020.12.02.0181 Scopus.
67. Jamel, H. O.; Mwaea, M. S.; Eidan, D. M.; Mahdi, M. A.; Jasim, L. S. Synthesis, Characterization, and Biological Evaluation of Nano Schiff Base Metal Complexes: Antibacterial and Anticancer Potential Against Breast Cancer (MCF-7) Cells. *Journal of Nanostructures* 2025, 15 (1), 88-107, Article. DOI: 10.22052/JNS.2025.01.009 Scopus.
68. Jamel, H. O.; Ali, M. H.; Eidan, D. M.; Mahdi, M. A.; Jasim, L. S. Synthesis, Spectroscopic Characterization and Biological Studies as an Anticancer of a Novel Schiff Base Ligand (LH) and Its Palladium (II) Complex Derived from Thiazole and Salicylaldehyde. *Journal of Nanostructures* 2024, 14 (2), 466-480, Article. DOI: 10.22052/JNS.2024.02.009 Scopus.